Yield loci for an anisotropic granular assembly

Luigi La Ragione[1,*] and Luc Oger[2]

[1]*School of Civil and Environmental Engineering, Cornell University, 14850 Ithaca, New York, USA*

[2]*Institut de Physique de Rennes, UMR CNRS-UR1 6251, Université de Rennes1, 263 Avenue du Général Leclerc, 35042 Rennes Cedex, France*

(Received 14 June 2012; revised manuscript received 24 August 2012; published 22 October 2012)

Yield loci of a granular material are derived in case of triaxial compression carried out at constant pressure. The theory is based upon a simple micromechanical model in which particles move according to an average, homogeneous deformation. We show how the presence of an inherent anisotropy in the aggregate (typical of laboratory samples due to depositional processes) produces a deviation of the yield loci in the stress space from the expected Mohr-Coulomb prediction. That is, when the compaction pressure in an anisotropic aggregate is increased, irreversibility associated with sliding between particles occurs and this will influence the yield function in the subsequent triaxial test. Numerical simulations support the theoretical result.

DOI: 10.1103/PhysRevE.86.041309 PACS number(s): 81.05.Rm, 62.20.fq, 62.20.fg

I. INTRODUCTION

Physical experiments in granular materials show the presence of inherent anisotropy and its influence on the mechanical behavior of the aggregate (e.g., Refs. [1–4]). Preferred orientation of particles, due to the depositional processes, characterizes this kind of anisotropy that turns out to affect the elastic response [5–8] as well as the shear stress and the volume change during any triaxial test (e.g., Refs. [9–13]). Here, we focus our attention on the correlation between inherent anisotropy and yield. In particular, the purpose of the paper is to show how inherent anisotropy can modify the yield loci of a granular assembly, typically a straight line in the stress space (the Mohr-Coulomb criterion). We do this in the context of the effective medium theory (EMT) supported by numerical simulations results.

The loading condition considered, after the specimen has been filled by raining particles, is an initial compression followed by shearing at constant pressure. In the initial compression, because of the inherent anisotropy, shear strain along with volume strain occur. Then particles can slide and this leads to a relaxation of the normal component of the contact displacement. Consequently, in the subsequent triaxial compression, sliding occurs earlier and this influences the yield function. That is, yield loci are not aligned along a straight line, as the Mohr-Coulomb criterion would have predicted, but they are along a curve with a reduction of the elastic range for the aggregate.

II. THEORY

We consider an ideal granular material made by a random aggregate of identical elastic, glass spheres with diameter D, shear modulus G, and Poisson's ratio ν. We refer to the typical process adopted in laboratory to prepare a granular sample, before any loading is applied, by raining particles through air under gravity. Consequently, the sample is characterized by an initial, inherent anisotropy whose vertical direction is **h**, while the isotropic plane is y_1-y_2. We focus on a dense aggregate, confined under a pressure p and then triaxial compressed at constant pressure. We assume a homogeneous, average deformation **E** and follow a previous analysis employed in Refs. [14,15]. The displacement **u** of a contact point relative to the particle center is given by $u_i = (D/2)E_{ij}\alpha_j$, where $\boldsymbol{\alpha}$ $(\sin\theta\cos\varphi, \sin\theta\sin\varphi, \cos\theta)$ is the unit vector directed from the particle center to the contact point, θ is the polar angle from the axis of symmetry **h**, and φ is the angle about this axis. The contact force, $F_i = P\alpha_i - T_i$, has a normal component $P = 2GD^2(\delta 6/D)^{3/2}/[9\sqrt{3}(1-\nu)]$ that follows the Hertz law, where δ is the normal component of the contact displacement, and a tangential component **T** with a bilinear behavior, an elastic resistance followed by a frictional sliding, where s is the tangential component of the contact displacement. So, $T_i = (2^{5/2}GD^{1/2})\delta^{1/2}s/(2-\nu)\hat{t}_i$ ($\hat{t}_i\alpha_i = 0$ with $\hat{t}_i$ in the direction of increasing θ), as long as contacting particles deform elastically; otherwise, when T reaches the limit value μP (μ is the interparticle friction coefficient) sliding occurs, and the tangential component of the contact force does not vary. This is quite a simplified model [16–18] that captures the main mechanism of the overall behavior of the aggregate. For the stress, we write

$$\sigma_{ij} = -\frac{nD}{2}\int_\Omega A(\alpha)\,F_i\alpha_j\,d\Omega, \tag{1}$$

where n is the number of particle per unit volume, Ω is the solid angle, and $A(\alpha)$ is the orientational distribution of contacts, defined so that the coordination number k, the average number of contacts per particle, is equal to $\int_\Omega A(\alpha)\,d\Omega$. The initial inherent anisotropy is accounted for in the model through an expression for the orientational distribution of contacts,

$$A(\alpha) = \frac{k}{4\pi}a(\varepsilon,\theta), \tag{2}$$

with $a(\varepsilon,\theta) = (1-\varepsilon) + 3\varepsilon(h_i\alpha_i)^2$ in which ε is the strength of the anisotropy [15,19].

A. Consolidation process

Before any shearing loading is applied, we compress the aggregate under a given pressure p with the deviatoric stress $q \equiv (\sigma_{11} - \sigma_{33})/2$ kept equal to zero. In this loading condition,

*Permanent address: Dipartimento di Scienze dell'Ingegneria Civile e Architettura, Politecnico di Bari, Via Re David 200, 70125 Bari, Italy.

because of the presence of an inherent anisotropy, shear strain, $\hat{\gamma} = -1/2\,(E_{11} - E_{33})$, occurs along with the volume strain, $\hat{\Delta} = -(2E_{11} + E_{33})$, and both the strains are positive. By definition, $\delta = -(D/2)E_{ij}\alpha_i\alpha_j$ and $s = (D/2)E_{ij}\alpha_j t_i$, or

$$\delta = \frac{D}{6}(\hat{\Delta} + 2\hat{\gamma} - 6\hat{\gamma}\cos^2\theta), \quad \text{and } s = -\frac{D}{2}\hat{\gamma}\sin 2\theta, \tag{3}$$

where the strain $\hat{\gamma}$ is a measure of the anisotropy. As the aggregate is compressed, both $\hat{\gamma}$ and $\hat{\Delta}$ increase. At contact level, the limit of elasticity is reached when the tangential component of the contact force, at a given θ, equals μP. Equivalently, $s = \hat{\mu}\delta$ (see Ref. [15] for more details), where $\hat{\mu} = \mu\,(2-\nu)\,/\,(3-3\nu)$, or, with Eq. (3),

$$g(\theta) = \frac{D}{2}\left[\hat{\gamma}\sin 2\theta - \frac{1}{3}\hat{\mu}(\hat{\Delta} + 2\hat{\gamma} - 6\hat{\gamma}\cos^2\theta)\right]. \tag{4}$$

We identify the angle θ_c where the sliding first occurs when $dg/d\theta = 0$ or

$$\cot 2\theta_c = \hat{\mu}. \tag{5}$$

Then, the value of the strains, $\hat{\gamma}^{(1)}$ and $\hat{\Delta}^{(1)}$, at which sliding first occurs, are obtained from the condition $g(\theta_c) = 0$, or

$$\frac{6\hat{\gamma}^{(1)}}{\hat{\Delta}^{(1)} + 2\hat{\gamma}^{(1)}} = \frac{2\hat{\mu}\sqrt{1+\hat{\mu}^2}}{1 + \hat{\mu}^2 + \hat{\mu}\sqrt{1+\hat{\mu}^2}}. \tag{6}$$

Given p, with $q = 0$, we have two equations to determine the unknowns $\hat{\Delta}$ and $\hat{\gamma}$. By definition, $p \equiv -\sigma_{kk}/3$, or

$$p = \frac{k\phi G}{9\pi\sqrt{3}(1-\nu)} \times \int_0^\pi a(\varepsilon,\theta)(\hat{\Delta} + 2\hat{\gamma} - 6\hat{\gamma}\cos^2\theta)^{3/2}\sin\theta d\theta, \tag{7}$$

with the solid volume fraction $\phi = n\pi D^3/6$; the shear stress is

$$q = \frac{3\phi k G}{\pi D^{1/2}2^{1/2}}\int_0^\pi a(\varepsilon,\theta)\delta^{1/2}\left[\frac{(3\cos^2\theta - 1)}{3(1-\nu)}\left(\frac{\delta}{D}\right) - \frac{3\hat{\gamma}}{2-\nu}\cos^2\theta\sin^2\theta\right]\sin\theta d\theta. \tag{8}$$

or, $q = 0$,

$$0 = \int_0^\pi a(\varepsilon,\theta)(\hat{\Delta} - 2\hat{\gamma} - 6\hat{\gamma}\cos^2\theta)^{1/2}\sin\theta \times\left[\frac{(\hat{\Delta} - 2\hat{\gamma} - 6\hat{\gamma}\cos^2\theta)(3\cos^2\theta - 1)}{9(1-\nu)} - \frac{6\hat{\gamma}\cos^2\theta\sin^2\theta}{(2-\nu)}\right]d\theta. \tag{9}$$

When the condition of Eq. (6) is met, $q = 0$ becomes

$$0 = \int_0^\pi a(\varepsilon,\theta)\left[\frac{(\hat{\Delta} - 2\hat{\gamma} - 6\hat{\gamma}\cos^2\theta)^{3/2}(3\cos^2\theta - 1)}{9(1-\nu)} - \frac{6\hat{\gamma}^{(1)}(\hat{\Delta}^{(1)} - 2\hat{\gamma}^{(1)} - 6\hat{\gamma}^{(1)}\cos^2\theta)^{1/2}\cos^2\theta\sin^2\theta}{(2-\nu)}\right] \times \sin\theta d\theta. \tag{10}$$

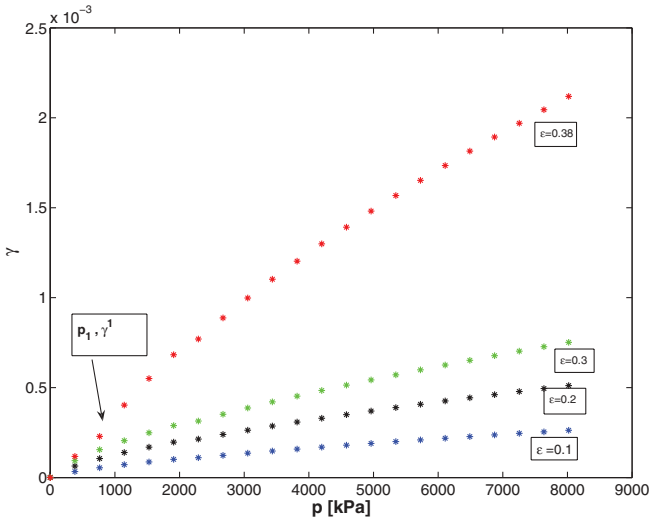

FIG. 1. (Color online) Shear strain versus pressure during the consolidation process for different value of ϵ. The case $\epsilon = 0$ corresponds to the x axis.

Note that when sliding first occurs, the tangential component of the contact force in q reaches its limiting value and it will not change as compression is continued [the second line in Eq. (10) does not vary with the strain]. This is how we relate the local yield (particle sliding) to the global yield function (yield loci). Certainly this is a rather simplified model to describe the impact of sliding into the mechanical response of the aggregate. However, numerical simulations (e.g., Ref. [20]) support this idea, even when a distribution of particle sliding is present; that is, initially only weakly loaded contacts slide and the overall response of the aggregate is marginally affected until stronger contacts slide. We conclude that the tangential component of the shear stress can be approximated with a bilinear elastic-perfectly plastic law.

The pressure preserves its expression, as it depends only on the normal component of the contact force. In the range of pressures of our interest, deletion does not occur although this can happen, first at $\theta = 0$, when $\delta = 0$. Therefore, given ε, the pressure p, and the condition $q = 0$, we determine $\hat{\gamma}$ and $\hat{\Delta}$. In Figs. 1 and 2 we plot, respectively, $\hat{\gamma}$ and $\hat{\Delta}$ as p increases, for different values of ε (the friction coefficient is $\mu = 0.2$). In the range $0 \leqslant \varepsilon \lesssim 0.4$, no sliding occurs during the isotropic compression and both $\hat{\gamma}$ and $\hat{\Delta}$ increase with p. For $\varepsilon \simeq 0.4$,

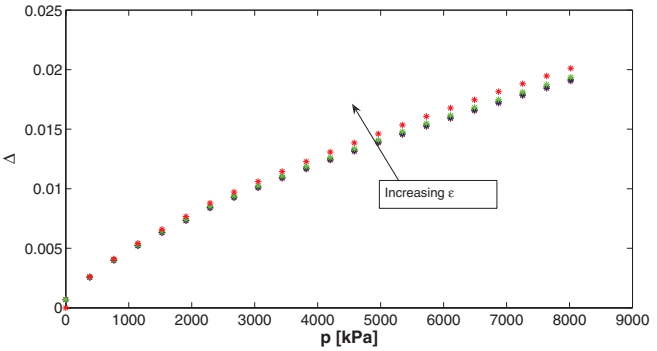

FIG. 2. (Color online) Volume strain versus pressure during the consolidation process for different value of ϵ.

inelasticity occurs, as the aggregate is compressed, at $p = p_1$, $\hat{\gamma} = \hat{\gamma}^{(1)}$, and $\hat{\Delta} = \hat{\Delta}^{(1)}$.

For pressures greater than p_1, while the behavior of $\hat{\Delta}$ resembles the trend seen at lower values of ε, $\hat{\gamma}$ experiences a clear variation. In fact, while for $p \leqslant p_1$, $\hat{\gamma}$ and $\hat{\Delta}$ are given as solutions of the Eqs. (7) and (9), when $p \geqslant p_1$, they are obtained from Eqs. (7) and (10). That is, in order to keep $q = 0$ when the tangential component of the contact force does not vary, γ associated with δ needs to increase. Consequently, δ, the normal component of the contact displacement that depends on both $\hat{\gamma}$ and $\hat{\Delta}$ [see Eq. (3)], is influenced by particle sliding. Inelasticity will affect not only the tangential component of the contact displacement, as naturally expected, but also the normal component δ. The problem is coupled; in the range of θ where δ decreases, because of the sharp increments of $\hat{\gamma}$ after $\hat{\gamma}^{(1)}$, the overlap between particles will be even smaller.

B. Triaxial compression at constant pressure: Yield loci

In the subsequent triaxial compression, we identify the yield loci in the stress space. It is arguable for an aggregate of particles to define a proper elastic limit, as, in general, weakly loaded particles may experience sliding before the heavily loaded one [20]. However, within a modeling approximation, we can attempt to distinguish the elastic from the plastic zone in the average sense, as pointed out in Sec. II A. For a granular material, this limit is often associated with the Mohr-Coulomb criterion, which is given by, in the q-p plane, a straight line through the origin, when cohesion is zero. However, as emphasized in Ref. [21], experiments suggest a "rounded drop-like shape" for the yield function that may find a justification with the presence of plastic deformation associated with crushing particles at relatively high confining pressure [22]. Here we suggest that the presence of inherent anisotropy, which is peculiar to many experimental samples, produces plastic deformations in the consolidation process that are responsible, in the subsequent triaxial test, for different shape of the yield loci.

For $p < p_1$, when $\varepsilon = 0.38$, and in all range of p when $\varepsilon < 0.38$, the elastic displacement is given by two contributions

$$u_i = \frac{D}{2}\tilde{E}_{ij}\alpha_j + \frac{D}{2}\hat{E}_{ij}\alpha_j, \tag{11}$$

where $\hat{\mathbf{E}}$ is the elastic strain associated with the isotropic compression

$$\hat{E}_{ij} = 2\hat{\gamma}h_i h_j - \tfrac{1}{3}(2\hat{\gamma} + \hat{\Delta})\delta_{ij}, \tag{12}$$

and $\tilde{\mathbf{E}}$ is the applied elastic strain in the triaxial compression

$$\tilde{E}_{ij} = 2\tilde{\gamma}h_i h_j - \tfrac{1}{3}(2\tilde{\gamma} + \tilde{\Delta})\delta_{ij}, \tag{13}$$

where $\tilde{\gamma}$ is now negative. In the triaxial compression test (now we label the quantity with subscript t), the normal component of the contact displacement δ_t and the tangential part s_t are

$$\delta_t = \frac{D}{6}[(\hat{\Delta} + \tilde{\Delta}) + 2(\hat{\gamma} + \tilde{\gamma}) - 6(\tilde{\gamma} + \hat{\gamma})\cos^2\theta] \tag{14}$$

and

$$s_t = -\frac{D}{2}(\tilde{\gamma} + \hat{\gamma})\sin 2\theta. \tag{15}$$

Again the yield condition, at contact level, is

$$\varphi \equiv |T| - \mu P = 0, \tag{16}$$

or in terms of the components of the contact displacement $s_t = \hat{\mu}\delta_t$ [with the minus sign in Eq. (15) as the sum of the two shear strains becomes negative]; following Eqs. (4)–(6), we obtain the relation between $\tilde{\gamma}$ and $\tilde{\Delta}$, for a given $\hat{\Delta}$ and $\hat{\gamma}$, when $\varphi = 0$

$$\frac{6(\tilde{\gamma} + \hat{\gamma})}{(\hat{\Delta} + \tilde{\Delta}) + 2(\tilde{\gamma} + \hat{\gamma})} = -\rho, \tag{17}$$

with

$$\cot 2\theta_c^t = -\hat{\mu} \tag{18}$$

and $\rho = 2\hat{\mu}\sqrt{1 + \hat{\mu}^2}/(1 + \hat{\mu}^2 - \hat{\mu}\sqrt{1 + \hat{\mu}^2})$. The shear stress along with the pressure, in case of triaxial compression, are given by Eqs. (7) and (8) with the normal and tangential component of the contact displacement given, respectively, by Eqs. (14) and (15). When sliding occurs, $\varphi = 0$, the yield loci are obtained in the stress space through the limit value of the ratio q/p, with Eq. (17) incorporated (see Appendix A):

$$\frac{q}{p} = \omega(\varepsilon, \mu). \tag{19}$$

For a given ε and μ, Eq. (19) represents a straight line in the p-q plane. That is, because no plastic deformation occurs during the consolidation process, the yield loci will depend only on the ratio of the stress components.

For $\varepsilon = 0.38$ and $p > p_1$, in the subsequent triaxial test, the elastic displacement is given by

$$u_i = \frac{D}{2}\tilde{E}_{ij}\alpha_j + \frac{D}{2}E_{ij}\alpha_j, \tag{20}$$

where

$$E_{ij} = 2\hat{\gamma}^{(1)}h_i h_j - \tfrac{1}{3}[6(\hat{\gamma}^{(1)} - \hat{\gamma})\cos^2\theta + 2\hat{\gamma} + \hat{\Delta}]\delta_{ij}. \tag{21}$$

The normal component of the contact displacement is given by Eq. (14) while the tangential part is

$$\check{s}_t = -\frac{D}{2}(\tilde{\gamma} + \hat{\gamma}^{(1)})\sin 2\theta. \tag{22}$$

The first yield, again, occurs when $\check{s}_t = \hat{\mu}\delta^t$ and the angle at which sliding first occurs is

$$\cot 2\check{\theta}_c^t = -\frac{\hat{\mu}(\tilde{\gamma} + \hat{\gamma})}{(\tilde{\gamma} + \hat{\gamma}^{(1)})}, \tag{23}$$

where now $\check{\theta}_c^t$ depends on the strain. As before, we determine the value of the strains during the triaxial compression, $\tilde{\gamma}$ and $\tilde{\Delta}$, associated with $\check{\theta}_c^t$, from the following equation:

$$\frac{-(\tilde{\gamma} + \hat{\gamma}^{(1)})^2}{\hat{\mu}\sqrt{(\tilde{\gamma} + \hat{\gamma}^{(1)})^2 + \hat{\mu}^2(\tilde{\gamma} + \hat{\gamma})^2}} = \frac{\hat{\Delta} + \tilde{\Delta}}{3} - (\tilde{\gamma} + \hat{\gamma})\left[\frac{1}{3} - \frac{\hat{\mu}(\tilde{\gamma} + \hat{\gamma})}{\sqrt{(\tilde{\gamma} + \hat{\gamma}^{(1)})^2 + \hat{\mu}^2(\tilde{\gamma} + \hat{\gamma})^2}}\right],$$

as we know $\hat{\gamma}^{(1)}, \hat{\gamma}$, and $\hat{\Delta}$. Unlike Eq. (17), the local yield condition now has a term that does not increase with the pressure, $\hat{\gamma}^{(1)}$. Again, the yield loci are obtained, in the stress space, through the ratio q/p where in the shear stress q, we now substitute $\hat{\gamma}$ with $\hat{\gamma}^{(1)}$ and where the pressure, Eq. (7), has

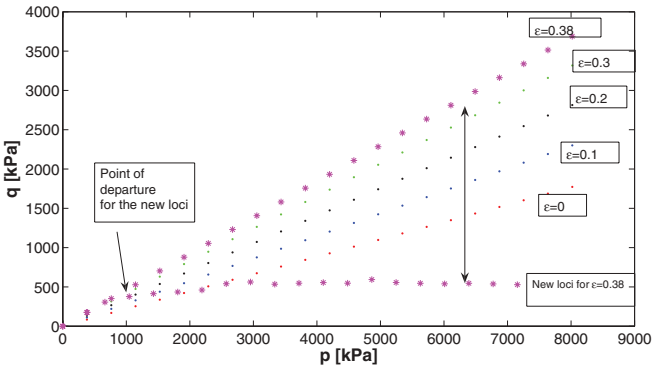

FIG. 3. (Color online) Yield loci in the stress plane for different values of ϵ. Both q and p are in kPa.

the normal component of the contact displacement given by Eq. (14). Consequently, we obtain (see Appendix B)

$$\frac{q}{p} = \chi(\mu, \varepsilon, \hat{\gamma}^{(1)}), \tag{25}$$

and it is evident how particle sliding in the consolidation process, through the parameter $\hat{\gamma}^{(1)}$, influences the yield loci.

In order to plot Eq. (25), we equate Eq. (7) with Eq. (27) as we consider a triaxial test at constant pressure and we then obtain an implicit relation between $\tilde{\Delta}$ and $\tilde{\gamma}$, as we know $\hat{\Delta}$, $\hat{\gamma}$, and $\hat{\gamma}^{(1)}$. In Fig. 3 we show the yield loci. Clearly, for $\varepsilon = 0.38$ and $p = p_1$, there is a departure from the straight line. Because of the plastic deformations in the initial state, the elastic limit in the triaxial compression is lower than what we would predict following the Mohr-Coulomb criterion.

Notice that when the local yield condition is independent of the strain, Eq. (18), the global yield function is a straight line, Eq. (19); conversely, when the local yield condition depends on the strain, Eq. (23), the yield loci are not along a straight line, Eq. (25). As underlined before, this is the consequence of the correlation between sliding and normal component of the contact displacement during the initial compression. That is, because of anisotropy, particles may slide during the initial compression loading and the tangential contact force may reach its limiting value; under further compression, only the normal component of the contact force will vary to keep $q = 0$ and, consequently, the elastic shear strain in the normal component of the contact displacement sharply increases; see Fig. 1. This leads to a further relaxation of the overlapping between particles for some contacts orientation. At the same time, the elastic component of the tangential displacement is not increased with p because of sliding [$\gamma^{(1)}$ is the limiting value, Eq. (22), when $\tilde{\gamma} = 0$]. Therefore, lower values for both components of the contact displacement allow to meet the local and, then, global yield condition earlier in the subsequent triaxial compression.

III. NUMERICAL SIMULATION

In order to test the prediction of the model we employ a numerical simulation based upon a classical discrete element method (DEM). The mechanical interaction is also taken from the literature and it is defined as the "Spring-Dashpot" model. We have used two different initial geometrical procedures to model two different structural anisotropies.

A. Anisotropic case

The preparation of the first sample is obtained by two consecutive procedures to mimic the real process of a box filling. The box filling is partially defined as under gravity (directional effect) [23]. The first layer is made by touching spheres sitting on the bottom wall. Then each new sphere is placed randomly on three already placed spheres. The choice is made considering stable contacts and the idea that its center is inside a given layer close to the upper surface. Each new sphere has its center inside an horizontal XY periodic box (i.e., the center is inside the box but the volume of the sphere can exit in one side in order to reappear in the opposite side). So, the packing is built layer by layer and the layer thickness is on the order 1/10 of the sphere radius. This Powell's algorithm will produce a rather dense solid volume fraction, ϕ, about 0.58–0.60. The sample contains 16 000 spheres with a mean radius ($D = 0.3$ mm) and a linear distribution of 5%. The material properties, typical of glass beads, are: $G = 17$ GPa, $\nu = 0.2$, and $\mu = 0.2$. The box has a square bottom with vertical dimension close as possible to obtain a cubic structure. We can already notice that in order to continue the compression process, we need to modify the lateral walls from the initial periodic conditions to some perfectly rigid walls at a distance larger than the initial box (i.e., plus almost one radius). This condition is defined by the fact that the walls do not have to overlap the spheres in order to work for the DEM following step. Indeed, the second step consists of a switching on the gravity field to generate the standard compression gradient due to the amount of grains present on top of the packing (seen as $\rho g H$ with ρ the density, g the gravity field, and H the packing height). Due to the difference of the local arrangements close to the walls, some small displacements can occur and produce a slight increase of the number of contacts behind each sphere. Indeed, the initial algorithm needs three contacts under each sphere and each contact belongs to two neighbors so the mean value for the coordination number will be six minus the wall perturbation (see Table I). Here we obtain a value of 5.47 before this gravitational step.

B. Isotropic case

In the isotropic case, the sample is prepared by using the classical Jodrey-Tory's algorithm [24]. A given series of seed of very small nonoverlapping spheres are generated inside a perfect cubic box with three-periodic boundary conditions. Then these spheres are slowly increased without overlap. When two or more spheres have some chances to overlap, their

TABLE I. Summary of the measures for the two numerical packings.

Packing case	Coordination number	Packing fraction	Fabric (ϵ)
Homogeneous	6.27	0.646	0.002
Gravitational	5.47	0.581	0.107

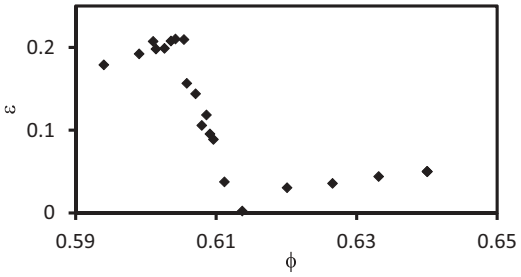

FIG. 4. Evolution of ϵ as a measure of the fabric tensor for the compression of the anisotropic packing up to the packing fraction equal to 0.64.

centers are moved apart according to the opposite direction of the overlaps in order to be just in contact. Each step is finished when all the possible overlaps are eliminated. Then we can continue to increase the sphere diameters. The program stops when we have reached a given ϕ or when the number of time steps has reached a given value. This program can generate very dense packing (ϕ close to 0.64) with a perfectly homogeneous disorder [24]. In the same manner as the previous case and in order to use the sample inside the three-axial compression program described later, we assumed also that the sample is inside a cubic box with all the walls just touching the external spheres (i.e., no overlaps). This constraint implies that the "real" packing fraction becomes lower (i.e., empty spaces close to the new walls due to the periodicity of the sphere volumes).

C. Geometrical measures of the two packing structures at $\phi = 0.64$

We measure the strength of anisotropy of the packings through the knowledge of the component of the fabric tensor $A_{ij} = \int A(\alpha)\alpha_i\alpha_j d\Omega$, or $A_{11} = A_{22} = 1/3 - 2\varepsilon/15$ and $A_{33} = 1/3 + 4\varepsilon/15$. In Table I we report the geometrical and structural measures for the two different packings. We note a difference in the initial configuration for the two series of samples either by their packing fraction or by their fabric measure (ϵ).

In order to start the triaxial test in the same conditions, we apply an isotropic compression to obtain the chosen $\phi \simeq 0.64$ in both cases. This compression is made under uniform strain constraint at low rate to allow local reorganization of contacts

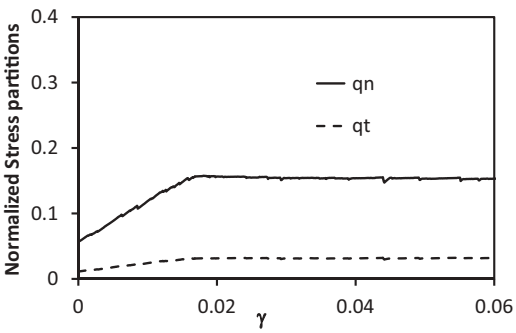

FIG. 5. Normalized deviatoric stress partition for the isotropic aggregate versus the deviatoric strain during the triaxial test (confining pressure $p = 800$ kPa).

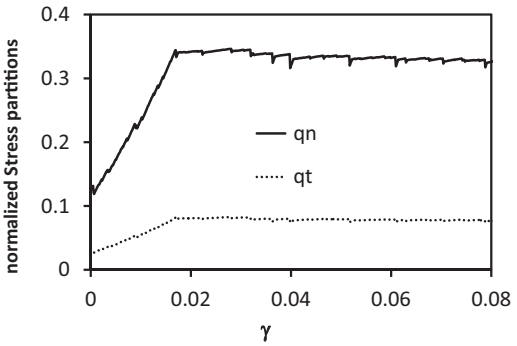

FIG. 6. Normalized deviatoric stress partition, for the anisotropic aggregate, versus the deviatoric strain during the triaxial test (confining pressures $p = 800$ kPa).

between grains. In the anisotropic packing we observe that this stage produces some changes in the local contacts network; the fabric measure decreases regularly from the value in Table I down to values close to 0.02–0.04 before increasing again (Fig. 4). Then we can conclude that the two packings remain different at the beginning of the triaxial test (at least ϵ has a factor 10 between the two cases). This difference is, in fact, higher if we only consider the forces that are really active in the aggregate. Therefore, in this consolidation process we see an evolution of the contact network that becomes negligible during the subsequent triaxial test. For the sake of simplicity, we have neglected this change in the theoretical model and the aggregate is characterized by its initial structure; however, this assumption seems to be more consistent in the triaxial test where the induced anisotropy is taken into account through the evolution of the contact stiffness and where the contact network stays almost unchanged, as seen in simulation.

D. Triaxial mechanical process and determination of yield loci

The isotropic and anisotropic aggregates have now the same ϕ and we continue with the classical three-axial uniform compression procedure in order to reach the requested confining pressure. At given pressure, we increase the wall displacement along the gravitational direction. We record the normal and tangential contact force contributions at 20 000 time steps each. As in Ref. [20], we distinguish the contribution of the normal component of the contact force on the deviatoric stress, q_N, from the tangential part, q_T. In Fig. 5 we plot the normalized

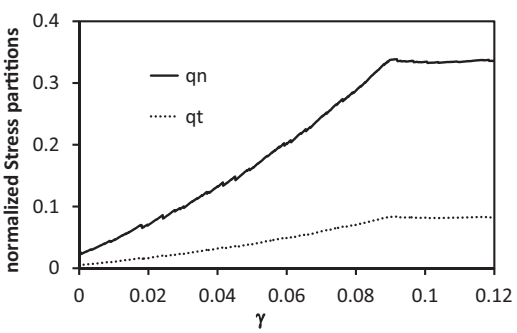

FIG. 7. Normalized deviatoric stress partition, for the anisotropic aggregate, versus the deviatoric strain during the triaxial test (confining pressures $p = 5000$ kPa).

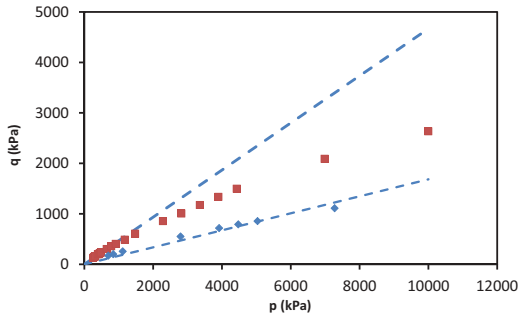

FIG. 8. (Color online) Numerical results for the anisotropic sample (square) and isotropic one (diamond). Both q and p are in kPa.

deviatoric stress partition for the isotropic aggregate, versus the deviatoric strain during the triaxial test for a confining pressure $p = 800$ kPa. There is no significant change as the pressure increases. In Figs. 6 and 7 we plot the normalized deviatoric stress partition, for the anisotropic aggregate, versus the deviatoric strain during the triaxial test for a confining pressure, respectively, of $p = 800$ kPa and $p = 5000$ kPa. Here we note substantial difference as the pressure increases.

When q_T becomes constant, we record the pair p and q. In Fig. 8 we plot the results. As the pressure increases, it is clear that the initial, anisotropic packing shows a different behavior than the expected Mohr-Coulomb trend that we confirm for the isotropic packing. Consistent with the well-known limitation of the EMT [25–27], a comparison between Figs. 3 and 8 shows the qualitative but not quantitative feature predicted by the model for different values of ϵ.

IV. CONCLUSION

In spite of the crude model employed that permits a simpler analysis, we show how inherent anisotropy may strongly influence the shape of the yield loci of a granular aggregate. It is possible to obtain inelasticity during the consolidation process that allows the aggregate to lower its elastic limit in the subsequent triaxial test. Numerical simulation supports the theoretical prediction although with a different ε. The difference can be explained by the fact that the average strain theory is a rather simple model and the local yield criterion, at contact level, is too crude.

ACKNOWLEDGMENTS

The authors are grateful to Jim Jenkins for fruitful discussions. L.L.R. is grateful to ONR Global (Grant No. N62909-12-1-4049) and COFIN 2008 (Italy) complex materials and structural models in advanced problems of engineering.

APPENDIX A

The shear stress along with the pressure, in case of triaxial compression, are given by

$$q = \frac{3\phi k G}{\pi D^{1/2} 2^{1/2}} \int_0^\pi a(\varepsilon,\theta)\delta_t^{1/2}\left[\frac{(3\cos^2\theta - 1)}{3(1-\nu)}\left(\frac{\delta_t}{D}\right) - \frac{3(\hat{\gamma} + \tilde{\gamma})}{2-\nu}\cos^2\theta \sin^2\theta\right]\sin\theta d\theta, \tag{A1}$$

$$p = \frac{Gk\phi}{\pi 9\sqrt{3}(1-\nu)} \int_0^\pi a(\varepsilon,\theta)\left(\frac{6\delta_t}{D}\right)^{3/2}\sin\theta d\theta. \tag{A2}$$

By substituting Eq. (17) in Eqs. (A1) and (A2), we obtain

$$\frac{q}{p} = \omega(\varepsilon,\mu), \tag{A3}$$

where

$$\omega(\varepsilon,\mu) = \frac{3}{4}\frac{\int_0^\pi a(\varepsilon,\theta) z^{3/2}(3\cos^2\theta - 1)\sin\theta d\theta}{\int_0^\pi a(\varepsilon,\theta) z^{3/2}\sin\theta d\theta} + \frac{27\rho\nu^*}{4}\frac{\int_0^\pi a(\varepsilon,\theta) z^{1/2}\cos^2\theta\sin^3\theta d\theta}{\int_0^\pi a(\varepsilon,\theta) z^{3/2}\sin\theta d\theta}, \tag{A4}$$

$z = 1 + \rho\cos^2\theta$ and $\nu^* = (1-\nu)/(2-\nu)$.

APPENDIX B

The stress ratio, at yield condition, is given by

$$\frac{q}{p} = \chi(\mu,\varepsilon,\hat{\gamma}^{(1)}),$$

where

$$\chi(\mu,\varepsilon,\hat{\gamma}^{(1)}) = \frac{3\int_0^\pi a(\varepsilon,\theta)\left(\frac{6\delta_t}{D}\right)^{3/2}(3\cos^2\theta - 1)\sin\theta d\theta}{4\int_0^\pi a(\varepsilon,\theta)\left(\frac{6\delta_t}{D}\right)^{3/2}\sin\theta d\theta} - \frac{81\nu^*}{2}(\tilde{\gamma} + \hat{\gamma}^{(1)})\frac{\int_0^\pi a(\varepsilon,\theta)\left(\frac{6\delta_t}{D}\right)^{1/2}\cos^2\theta\sin^2\theta\sin\theta d\theta}{\int_0^\pi a(\varepsilon,\theta)\left(\frac{6\delta_t}{D}\right)^{3/2}\sin\theta d\theta}. \tag{B1}$$

[1] J. R. F. Arthur and B. K. Menzies, Geotechnique **22**, 115 (1972).
[2] R. Kuwano and R. J. Jardine, Geotechnique **52**, 727 (2002).
[3] A. Ezaoui and H. Di Benedetto, Geotechnique **59**, 621 (2009).
[4] Y. Khidas and X. Jia, Phys. Rev. E **81**, 021303 (2010).
[5] Y. C. Chen, I. Ishibashi, and J. T. Jenkins, Geotechnique **38**, 25 (1988).
[6] B. Cambou, Ph. Dubujet, and C. Nouguier-Lehon, Mech. Mater. **36**, 1185 (2004).
[7] C. S. Chang and Z.-Y. Yin, J. Eng. Mech. **136**, 830 (2010).
[8] L. La Ragione and V. Magnanimo, Phys. Rev. E **85**, 031304 (2012).
[9] M. Oda, Soils Foundations **12**, 17 (1972).
[10] X. S. Li, and Y. F. Dafalias, J. Geotech. Geoenviron. Eng. ASCE **128**, 868 (2002).
[11] S. Luding, J. Phys.: Condens. Matter. **17**, S2623 (2005).
[12] Z. X. Yang, X. S. Li, and J. Yang, Geotechnique **58**, 237 (2008).
[13] M. Kuhn, Mech. Mater. **42**, 827 (2010).

[14] J. T. Jenkins, in *Micromechanics of Granular Materials*, edited by M. Satake and J. T. Jenkins (Elsevier, Amsterdam, 1988), pp. 245–252.
[15] J. T. Jenkins and O. D. L. Strack, Mech. Mater. **16**, 25 (1993).
[16] D. Elata and J. G. Berryman, Mech. Matls. **24**, 229 (1996).
[17] R. D. Mindlin and H. Deresiewicz, J. Appl. Mech. **20**, 327 (1953).
[18] D. L. Johnson and A. N. Norris, J. Mech. Phys. Sol. **45**, 1025 (1996).
[19] K. Kanatani, Int. J. Eng. Sci. **22**, 149 (1984).
[20] C. Thornton and S. J. Antony, Philos. Trans. R. Soc. London A **356**, 2763 (1998).
[21] S. Krenk, Int. J. Solids Struct. **37**, 6343 (2000).
[22] M. Taiebat and Yannis F. Dafalias, Int. J. Geom. **161**, 161 (2010).
[23] M. J. Powell, Powder Technol. **25**, 45 (1980).
[24] W. S. Jodrey and E. M. Tory, Powder Technol. **30**, 111 (1981).
[25] M. A. Koenders, Acta Mech. **70**, 31 (1987).
[26] J. Jenkins, D. Johnson, L. La Ragione, and H. A. Makse, J. Mech. Phys. Solids **53**, 197 (2005).
[27] H. A. Makse, N. Gland, D. L. Johnson, and L. Schwartz, Phys. Rev. Lett. **83**, 5070 (1999).